# Optical, morphological, structural, electrical, molecular orientation, and electroluminescence characteristics of organic semiconductor films prepared at various deposition rates

Toshinori Matsushima [a], Koutaro Shiomura [a], Shigeki Naka [b], Hideyuki Murata [a,*]

[a] *School of Materials Science, Japan Advanced Institute of Science and Technology, 1−1 Asahidai, Nomi, Ishikawa 923−1292, Japan*

[b] *Graduate School of Science and Engineering, University of Toyama, 3190 Gofuku, Toyama 930−8555, Japan*

*Keywords:* Organic light−emitting diode, High deposition rate, Photoluminescence quantum yield and lifetime, Time−of−flight charge carrier mobility, Molecular orientation

## ABSTRACT

Extremely high deposition rates of ≈7200 nm $s^{-1}$ for *N*,*N*′−diphenyl−*N*,*N*′−bis(1−naphthyl)−1,1′−biphenyl−4,4′−diamine (α−NPD) and of

≈1700 nm $s^{-1}$ for tris(8−hydroxyquinoline)aluminum ($Alq_3$) are found to be possible by controlling source−substrate distances and crucible temperatures. Shapes of ultraviolet−visible absorption spectra and photoluminescence (PL) spectra, atomic force microscope images, X−ray diffraction patterns, PL quantum yields, PL lifetimes, and PL radiative decay rates of the films remain independent of the deposition rates ranging from 0.01 to 1000 nm $s^{-1}$. On the other hands, hole currents of hole−only α−NPD devices increase ≈3 times while electron currents of electron−only $Alq_3$ devices decrease by ≈1/60 as the deposition rates are increased from 0.01 to 10 nm $s^{-1}$. The increase in hole current is confirmed to arise from an increase in hole mobility of α−NPD measured using a time−of−flight technique. The increase in hole moility is probably due to a parallel orientation of an electronic transition moment of α−NPD at the higher deposition rates. Moreover, the three orders of magnitude increase in deposition rate from 0.01 to 10 nm $s^{-1}$ of α−NPD and $Alq_3$ results in a relatively small increase in voltage of ≈15% and a decrease in external quantum efficiency of ≈30% in organic light−emitting diodes (OLEDs). The reduction of the OLED performance is attributable to the marked decrease in electron current relative to the slight increase in hole current, indicating a decrease in charge balance factor at the higher deposition rates.

* Corresponding author. Tel.: +81 761 51 1531; fax: +81 761 51 1149

*E-mail address*: murata-h@jaist.ac.jp (H. Murata)

## 1. Introduction

A vacuum thermal deposition technique used to manufacture multilayer organic light−emitting diodes (OLEDs) based on small molecules [1] is inherently time−consuming, resulting in the overall cost of manufacturing OLEDs greater than that of manufacturing widely commercialized liquid crystal displays and plasma panel displays. Constructing the multilayer OLED structure at a high deposition rate is suggested to be an alternative way to reduce the tact time [2]. The deposition rates of organic layers embedded into OLEDs are typically less than ≈0.1 nm $s^{-1}$ and are considered one of the key factors affecting performance of OLEDs. Indeed, Chen and coworkers have shown that electron mobilities of tris(8−hydroxyquinoline)aluminum ($Alq_3$) decrease and power consumption of OLEDs increases by a small increase in deposition rate of $Alq_3$ from 0.2 to 0.7 nm $s^{-1}$ [3]. Lie and coworkers have demonstrated that electroluminescence (EL) efficiencies and operational lifetimes of OLEDs are improved with increasing deposition rates of bis(10−hydroxybenzo[h]qinolinato)beryllium ($Bebq_2$) from 0.03 to 1.3 nm $s^{-1}$ [4]. The variation range of the deposition rates previously used to investigate device performance is less than two orders of magnitude [3−7]. There has been still a lack of understanding that how optical and electrical characteristics of organic films as well as

performance of OLEDs are affected when the deposition rates are widely changed by several orders of magnitude. In this study, we investigate the wide dependence of the deposition rates of *N*,*N*′−diphenyl−*N*,*N*′−bis(1−naphthyl)−1,1′-biphenyl−4,4′−diamine (α−NPD) and $Alq_3$ on their optical, morphological, structural, electrical, molecular orientation, and EL characteristics.

## 2. Experimental details

Glass substrates coated with a 150 nm layer of indium tin oxide (ITO) and fused silica substrates were cleaned using conventional ultrasonication, followed by ultraviolet−ozone treatment. Organic films were vacuum−deposited on the substrates under a pressure of $\approx 10^{-4}$ Pa using fused silica or carbon crucibles as deposition sources. In our deposition setup, temperatures of the crucibles and distances between the crucible and the substrate were controllable ranging in temperature from room temperature to 400 ºC and ranging in distance from 18 to 0.5 cm. Therefore, the deposition rates could be six orders of magnitude changed from 0.001 to over 1000 nm $s^{-1}$ by controlling the source−substrate distances and the crucible temperatures. The deposition rates were monitored using a carefully calibrated quartz crystal microbalance.

For optical, morphological, and structural characterizations, the films of α−NPD and $Alq_3$ were vacuum−deposited on the fused silica substrates at the deposition rates ranging from 0.01 to 1000 nm $s^{-1}$ by controlling the source−substrate distances as well as the crucible temperatures. The film thicknesses were set at 100 nm using the quartz crystal microbalance in the case of the low deposition rates less than 10 nm $s^{-1}$. When the high deposition rates of 100 and 1000 nm $s^{-1}$ were used, the resulting film thicknesses were widely varied depending on the films due to extremely short deposition times (for examples, 1 s for 100 nm $s^{-1}$ and 0.1 s for 1000 nm $s^{-1}$ to obtain 100 nm films). Thus, we prepared more than 10 films at the deposition rates of 100 and 1000 nm $s^{-1}$ and measured their film thicknesses by stylus profilometry (Dektak 3030, Veeco). The measured film thicknesses ranged from 90 to 750 nm. Among the films, we chose the films having the thicknesses ranging from 100 to 150 nm for the optical, morphological, and structural characterizations. The ultraviolet−visible (UV−vis) absorption spectra, the photoluminescence (PL) spectra, the PL quantum yields, the PL lifetimes, the surface morphologies, and the X−ray diffraction (XRD) patterns of the films were measured respectively by using a V670 spectrometer (JASCO), a FP−6500 spectrometer (JASCO), a C9920 absolute PL quantum yield measurement system (Hamamatsu Photonics), a fluorocube spectrometer (Horiba Jobin Yvon), a SPA400

atomic force microscope (AFM) (Seiko), and a M18XHF X−ray diffractometer (MAC Science). The scan speeds of wavelength for the absorption and PL spectra were set at 100 nm $s^{-1}$. The wavelengths of excitation light for the PL spectra and quantum yields were set at 320 nm for α−NPD and 370 nm for $Alq_3$. A dynamic−force mode and a standard uncoated cantilever (SI−DF20) were used for the AFM images. The transient PL curves of α−NPD and $Alq_3$ at wavelengths of their absorption maxima were measured under 378 nm pulse excitation light to estimate the PL lifetimes. The XRD patterns were measured using a conventional $2\theta/\theta$ technique with a CuKα X−ray source ($\lambda$=1.54 Å). All measurements were conducted at room temperature.

The hole−only and electron−only device structures were glass substrate/ITO anode (150 nm)/$MoO_3$ (0.75 nm)/α-NPD (200 nm)/$MoO_3$ electron−blocking layer (10 nm) [8]/Al cathode (100 nm) and glass substrate/ITO anode (150 nm)/2,9−dimethyl−4,7−diphenyl−1,10−phenanthroline (BCP) hole−blocking layer (30 nm) [9]/$Alq_3$ (200 nm)/LiF electron−injection layer (0.5 nm) [10]/Al cathode (100 nm), respectively [see the device structures shown in Figs. 1(a) and 1(b)]. Also, the OLED structure was glass substrate/ITO anode (150 nm)/$MoO_3$ buffer layer (0.75 nm) [8]/α−NPD hole−transport layer (60 nm) [10]/$Alq_3$ light−emitting electron−transport

layer (65 nm) [1]/LiF electron−injection layer (0.5 nm)/Al cathode (100 nm) as shown in Fig. 1(c). To fabricate the devices, the deposition rates of α−NPD and $Alq_3$ were changed from 0.01 to 10 nm $s^{-1}$ by controlling the crucible temperatures while the deposition rates of the other layers were set at constant: 0.05 nm $s^{-1}$ for $MoO_3$, 0.01 nm $s^{-1}$ for LiF, 0.5 nm $s^{-1}$ for Al, and 0.1 nm $s^{-1}$ for BCP. The source−substrate distance of 18 cm was used and the maximum deposition rate was limited to 10 nm $s^{-1}$ to ensure film uniformity and final film thickness. The current density−voltage−external quantum efficiency characteristics and the EL spectra of the devices were measured as previously reported [8,9].

## 3. Results and discussion

The deposition rate−crucible temperature characteristics of α−NPD and $Alq_3$ with the different source−substrate distances are shown in Figs. 2(a) and 2(b), respectively. The extremely high deposition rates of ≈7200 nm $s^{-1}$ for α−NPD (at a temperature of 400 ºC and a distance of 1 cm) and of ≈1700 nm $s^{-1}$ for $Alq_3$ (at a temperature of 400 ºC and a distance of 0.5 cm) are found to be possible. The temperature of the substrate surface during the α−NPD deposition is recorded using a tiny thermocouple with a diameter of 50 μm which is mechanically fixed on the substrate surface [Fig. 2(c)]. The

use of the higher deposition rates and the shorter source−substrate distances results in the more rapid increase in substrate temperature due to heating caused by a hot α−NPD vapor and a radiant ray from the crucible. The deposition times needed to obtain the 100 nm films are 10000 s for 0.01 nm $s^{-1}$, 100 s for 1 nm $s^{-1}$, 10 s for 10 nm $s^{-1}$, and 0.1 s for 1000 nm $s^{-1}$. Within the deposition times, the substrate temperature increases by only 2−6 ºC, so that the small variation of the substrate temperature would be less influential for the film and device characteristics.

The increase in crucible temperature to obtain the high deposition rates may give rise to a question that whether molecules are thermally decomposed or not during the film deposition. Thus, the resulting films obtained at various crucible temperatures are analyzed by means of high performance liquid chromatography (1100LC, Agilent) and mass spectrometry (JMS−SX102A, JEOL). If molecules are thermally decomposed, it is supposed that additional peaks are observed in the chromatography and mass spectra of the high−deposition−rate films when compared with the source powders. However, there is no detectable difference in their chromatography spectra between the films and the source powders. The chromatography ensures the purity of the films greater than 99%. In the mass spectra, we see several peaks originating from some ionized parts of

molecules. The peak positions and the peak numbers of the mass spectra are similar among the films, but the relative peak intensities are slightly different depending on the films. Although we are not still on the place to decide whether thermally decomposed species is present or not, we can only speculate from the results that the amount of thermally decomposed species is not so large at the high crucible temperatures.

The cross sectional profiles of the films of α−NPD and $Alq_3$ prepared with the high deposition rate of 500 nm $s^{-1}$, the source−substrate distance of 1 cm, and the deposition time of 30 s are measured using the stylus profilometry. The typical profiles shown in Figs. 3(a) and Fig. 3(b) display a flat−top region from which the film thicknesses are calculated to be 14.6±0.2 μm for α−NPD and 14.0±0.7 μm for $Alq_3$ respectively. The calculated thicknesses almost correspond to the expected thickness (500 nm $s^{-1}$×30 s=15 μm). The AFM images and the optical spectra presented later are measured in the flat−top regions of the high−deposition−rate films.

There is no obvious change in AFM image and surface roughness of α−NPD and $Alq_3$ prepared at the deposition rates ranging from 0.01 to 1000 nm $s^{-1}$. The representative AFM images of the films of α−NPD and $Alq_3$ prepared at the deposition

rates of 0.01 and 1000 nm $s^{-1}$ are shown in Figs. 3(c)−(f). The films of α−NPD and $Alq_3$ have a small grain structure with grain diameters less than 50 nm. The average surface roughnesses of the films are estimated to be 0.38±0.12 nm (α−NPD) and 0.36±0.09 nm ($Alq_3$) from the AFM images of all films, which are slightly larger than that of 0.28±0.02 nm obtained from the optically polished quartz substrates. Moreover, results of the XRD measurement using a conventional $2\theta/\theta$ technique revealed that the prepared films of α−NPD and $Alq_3$ had no diffraction peaks whereas there were intense diffraction peaks from source powders of α−NPD and $Alq_3$ and vacuum−deposited pentacene thin films [11], indicating amorphous film formation [7,11].

The representative UV−vis absorption spectra of the films of α−NPD and $Alq_3$ prepared at the deposition rates of 0.01 and 1000 nm $s^{-1}$ are shown in Figs. 4(a) and 4(b), respectively. The absorption coefficients of α−NPD and $Alq_3$ are calculated by dividing the peak absorbances at ≈350 nm (α−NPD) and at ≈400 nm ($Alq_3$) by the actual film thicknesses measured by the stylus profilometry [Figs. 4(c) and 4(d)]. The shapes of the UV−vis absorption spectra are independent of the deposition rates and agree with those of previously reported spectra [12−14]. Despite the unchanged spectral shapes, the absorption coefficients gradually decrease by ≈15% (α−NPD) and ≈30%

($Alq_3$) as the deposition rates are increased from 0.01 to 1000 nm $s^{-1}$. The decrease in absorption coefficient is indicative of a decrease in density of molecules, which may be caused by unstable configuration of molecules in the films prepared at the higher deposition rates.

The representative PL spectra of the films of α−NPD and $Alq_3$ prepared at the deposition rates of 0.01 and 1000 nm $s^{-1}$, the PL quantum yield−deposition rate characteristics, the PL lifetime−deposition rate characteristics, and the PL radiative decay rate−deposition rate characteristics are shown in Fig. 5. The shapes of the PL spectra and the obtained optical parameters remain independent of the deposition rates as well and are in agreement with those reported previously [15−17]. Moreover, since the two PL quantum yield−deposition rate curves obtained using the different source−substrate distances and crucible temperatures are well overlapped, the films have less exciton quencher generated by thermal decomposition.

The current density−voltage characteristics of the hole−only α−NPD devices and the electron−only $Alq_3$ devices are shown in Figs. 6(a) and 6(b), respectively (see the device structures shown in Figs. 1(a) and 1(b)). Also, the current density−deposition rate

characteristics are shown in Fig. 6(c). No EL is observed from the devices during the current density−voltage measurements, indicating completely unipolar current flow. When the deposition rates are increased from 0.01 to 10 nm $s^{-1}$, the current densities of the electron−only $Alq_3$ devices decrease by ≈1/60, which agree with the decrease in electron mobility of $Alq_3$ reported in Ref. [3]. On the other hands, the current densities of the hole−only α−NPD devices reversely increase ≈3 times. This result is contradictory to our expectation that the decrease in density of molecules [Figs. 4(c) and 4(d)] lowers probability of hopping transport between neighboring molecules.

To investigate the increase in hole current observed in the α−NPD devices, hole mobilities of α−NPD films prepared at various deposition rates are analyzed from a glass substrate/ITO (150 nm)/Al (20 nm)/α−NPD (3000 nm)/Al (200 nm) structure using a time−of−flight (TOF) technique as previously reported in Ref. [18]. The TOF hole transients of α−NPD measured at an electric field of $2.7\times10^5$ V $cm^{-1}$ are shown in Fig. 7(a). The transient currents somehow increase with time even if excitation light powers are varied. Then, the transient currents suddenly drop because holes reach the counter electrode. The hole transit time ($t_{TR}$) is estimated from a change in slope in the transients. The hole mobilities ($\mu$) of α−NPD under a wide range of electric fields are

determined from the relationship $\mu=L^2/(t_{TR}V)$ [18], where $L$ is the cathode−anode spacing and $V$ is the voltage. All α−NPD films have field−dependent hole mobilities ($\mu$) as shown in Fig. 7(b). The field−dependent hole mobilities are expressed as $\mu=\mu_0\exp(\beta E^{0.5})$ [3,18], where $\mu_0$ is the zero field hole mobility, $\beta$ is the field dependence parameter, and $E$ is the electric field. The zero field hole mobilities of α−NPD are found to slightly increase as the deposition rates are increased [Fig. 6(c)], but the field dependence parameters remain constant for all films ($\approx 1.4\times10^{-3}$ $cm^{0.5}$ $V^{-0.5}$). The obtained values are similar to those previously reported ($\mu_0=4.0\times10^{-4}$ $cm^2$ $V^{-1}$ $s^{-1}$ and $\beta=1.1\times10^{-3}$ $cm^{0.5}$ $V^{-0.5}$) [18]. Since the hole mobilities of α−NPD are changed in the manner similar to the current densities of the hole−only α−NPD devices [Fig. 6(c)], the increase in hole current arises from the increase in hole mobility.

It has been reported recently that a molecular orientation occurs when growth conditions of organic films are changed [19]. Thus, the films of α−NPD and $Alq_3$ are vacuum−deposited on the fused silica substrates at the deposition rates of 0.01, 0.1, 1, and 10 nm $s^{-1}$ and their molecular orientations are evaluated using polarized absorption spectra under normal and oblique (45°) light incidence [11] [Figs. 8(a) and 8(b)]. The absorption of all $Alq_3$ films is unpolarized under both normal and oblique incidence,

indicating that the $Alq_3$ films are optically random in every direction [Fig. 8(b)]. There is no polarized absorption from the α−NPD films under the normal incidence as well [Fig. 8(a)], indicating that α−NPD molecules are in−plane random. However, for the oblique incidence, the *p*−polarized absorbance is larger than the *s*−polarized absorbance in the 0.01 nm $s^{-1}$ α−NPD film. And the *p*−polarized and *s*−polarized absorbances are gradually reversed as the deposition rates are increased from 0.01 to 10 nm $s^{-1}$. The molecular orientation of α−NPD is somewhat induced using the higher deposition rates in the manner that the electronic transition moment direction is changed from normal to parallel to the substrate. One tends to consider formation of a random molecule structure at the higher deposition rates due to short−range surface migration of molecules, but the obtained result is somehow opposite. The change in the molecular orientation of α−NPD could be related to the increase in hole current and hole mobility [Fig. 6(c)]. Moreover, the transition moment orientation parallel to the substrate increases the absorbance by ≈15% because molecules with the parallel oriented transition moment can absorb the normal−incidence light more strongly than the oblique−incidence light. Thus, the decrease in absorption coefficient of α−NPD (≈15%) is slower than that of $Alq_3$ (≈30%) [Figs. 4(c) and 4(d)], probably due to the parallel transition moment orientation.

The current density−voltage and external quantum efficiency−current density characteristics of the OLEDs prepared using the different deposition rates are shown in Figs. 9(a) and 9(b), respectively [see the device structure shown in Fig. 1(c)]. The drive voltages and the external quantum efficiencies at the current densities of 1, 10, and 100 mA $cm^{-2}$ are plotted versus the deposition rates in Fig. 9(c). We observe an increase in drive voltage and a decrease in external quantum efficiency as the deposition rates of α−NPD and $Alq_3$ are increased [Fig. 9(c)]. Shapes of EL spectra of all OLEDs (originating from electrically excited $Alq_3$) remain independent of the deposition rates, indicating that a carrier recombination zone is probably pinned near the α-NPD/$Alq_3$ interface. The maximum external quantum efficiency at the deposition rate of 0.1 nm $s^{-1}$ and the shapes of the EL spectra correspond well with those previously reported [15,16].

The external quantum efficiencies ($\eta_{EXT}$) can be given by the equation [20,21], $\eta_{EXT}=\eta_{OUT}\eta_{E/H}\eta_{EXC}\eta_{PL}$, where $\eta_{OUT}$ is the light out−coupling efficiency, $\eta_{E/H}$ is the charge balance factor, $\eta_{EXC}$ is the efficiency of single or triplet exciton generation, and $\eta_{PL}$ is the PL quantum yield. Since the exciton generation efficiency is basically fixed at 0.25 for fluorescence materials [21] and the light out−coupling efficiency is assumed to

be independent of the deposition rates due to the unchanged EL spectra, the observed decrease in external quantum efficiency is therefore attributable to a decrease in either charge balance factor or PL quantum yield. Since the PL quantum yields are unchanged in the whole deposition rate region as can be seen in Figs. 5(c) and 5(d), we can conclude that the PL quantum yields cause no influence on the external quantum efficiencies of the OLEDs. On the other hands, the opposite changes in the current density−deposition rate characteristics of the single−carrier devices in Fig. 6(c) suggest that the increase in drive voltage and the decrease in external quantum efficiency of the OLEDs are caused by the marked decrease in electron current relative to the slight increase in hole current, meaning that the decrease in charge balance factor at the higher deposition rates.

## 4. Summary

Optical, morphological, structural, electrical, molecular orientation, and EL characteristics of organic films depending on organic deposition rates are investigated. Shapes of UV−vis absorption spectra and PL spectra, AFM images, XRD patterns, PL quantum yields, PL lifetimes, and PL radiative decay rates of films of α−NPD and $Alq_3$ remain independent of the deposition rates ranging from 0.01 to 1000 nm $s^{-1}$. On the

other hands, hole currents of hole−only α−NPD devices increase ≈3 times while electron currents of electron−only $Alq_3$ devices decrease by ≈1/60 when the deposition rates are increased from 0.01 to 10 nm $s^{-1}$. The increase in hole current is confirmed to arise from an increase in hole mobility of α−NPD measured using a TOF technique. The increase in hole mobility is probably due to a parallel orientation of an electronic transition moment of α−NPD at the higher deposition rates. Moreover, we find that drive voltages increase by ≈15% and external quantum efficiencies decrease by ≈30% for OLEDs when the deposition rates of α−NPD and $Alq_3$ are increased from 0.01 to 10 nm $s^{-1}$. From the results of the PL quantum yields and the current density−voltage characteristics of the single−carrier devices, we can conclude that the decrease in external quantum efficiency is attributable to the decrease in electron current relative to the increase in hole current, which leads to a decrease in charge balance factor. Since the decrease in electron current is more pronounced than the increase in hole current, the drive voltages of the OLEDs are assumed to increase when the higher deposition rates are used. This finding opens a way to fabrication of high−performance OLEDs at high deposition rates if organic layers showing enhanced charge transport like α−NPD can be used in OLEDs.

**Acknowledgement**

The authors are grateful to Prof. Hiroyuki Okada (University of Toyama) for useful discussion and Dr. Hidetoshi Fujimura (FUJIFILM CO.) for measurements of mass spectrometry and liquid chromatography. This work is supported by Grants−in−Aid for Scientific Research (Grant Nos. 21760005, 20241034, and 20108012). Part of this work is based on “Development of the next generation large−scale organic EL display basic technology (Green IT Project)” with New Energy and Industrial Technology Development Organization (NEDO).

**References**

[1] C. W. Tang, S. A. VanSlyke, Appl. Phys. Lett. 51 (1987) 913.

[2] E. Matsumoto, S. Maki, Y. Yanagi, T. Nishinori, Y. Kondo, Y. Kishi, J. Kido, Society for Information Display International Symposium, Digest of Technical Papers, 34 (2003) 1423.

[3] B. J. Chen, W. Y. Lai, Z. Q. Gao, C. S. Lee, S. T. Lee, W. A. Gambling, Appl. Phys. Lett. 75 (1999) 4010.

[4] S.-W. Liu, C.-C. Lee, C.-H. Wang, J.-H. Lee, C.-T. Chen, J.-K. Wang, Chem. Phys. Lett. 474 (2009) 207.

[5] Y. Qiu, D. Q. Zhang, J. Qiao, Y. Shao, Synth. Met. 110 (2000) 241.

[6] H. Mu, H. Shen, D. Klotzkin, Solid-State Electron. 48 (2004) 2085.

[7] P.-T. Lee, T.-Y. Chang, S.-Y. Chen, Org. Electron. 9 (2008) 916.

[8] T. Matsushima, G.-H. Jin, H. Murata, J. Appl. Phys. 104 (2008) 054501.

[9] T. Matsushima, M. Takamori, Y. Miyashita, Y. Honma, T. Tanaka, H. Aihara, H. Murata, Org. Electron. 11 (2010) 16.

[10] L. S. Hung, C. W. Tang, M. G. Mason, Appl. Phys. Lett. 70 (1997) 152.

[11] T. Matsushima, H. Murata, Appl. Phys. Lett. 98 (2011) 253307.

[12] J. Kido, T. Matsumoto, Appl. Phys. Lett. 73 (1998) 2866.

[13] T. Matsushima, Y. Kinoshita, H. Murata, Appl. Phys. Lett. 91 (2007) 253504.

[14] D.-S. Leem, H.-D. Park, J.-W. Kang, J.-H. Lee, J. W. Kim, J.-J. Kim, Appl. Phys. Lett. 91 (2007) 011113.

[15] G. Sakamoto, C. Adachi, T. Koyama, Y. Taniguchi, C. D. Merritt, H. Murata, Z. H. Kafafi, Appl. Phys. Lett. 75 (1999) 766.

[16] T. Dobbertin, M. Kroeger, D. Heithecker, D. Schneider, D. Metzdorf, H. Neuner, E. Becker, H.-H. Johannes, W. Kowalsky, Appl. Phys. Lett. 82 (2003) 284.

[17] Y. Kawamura, H. Sasabe, C. Adachi, Jpn. J. Appl. Phys. 43 (2004) 7729.

[18] S. Naka, H. Okada, H. Onnagawa, Y. Yamaguchi, T. Tsutsui, Synth. Met. 111−112 (2000) 331.

[19] D. Yokoyama, Y. Setoguchi, A. Sakaguchi, M. Suzuki, C. Adachi, Adv. Funct. Mater. 20 (2010) 386.

[20] T. Tsutsui, Mater. Res. Soc. Bull. 22 (1997) 39.

[21] M. A. Baldo, D. F. O'Brien, M. E. Thompson, S. R. Forrest, Phys. Rev. B 60 (1999) 14422.

**Figure captions**

**Fig. 1.** Schematic structures of (a) hole−only devices, (b) electron−only devices, and (c) OLEDs.

**Fig. 2.** Deposition rate−crucible temperature characteristics of (a) α−NPD and (b) $Alq_3$ with different source−substrate distances and (c) substrate temperature−time characteristics measured during α−NPD deposition.

**Fig. 3.** Cross sectional profiles of films of (a) α−NPD and (b) $Alq_3$ prepared with deposition rate of 500 nm $s^{-1}$, source−substrate distance of 1 cm, and deposition time of 30 s and AFM images of α−NPD prepared at deposition rates of (c) 0.01 and (d) 1000 nm $s^{-1}$ and of $Alq_3$ prepared at deposition rates of (e) 0.01 and (f) 1000 nm $s^{-1}$.

**Fig. 4.** UV-vis absorption spectra of (a) α−NPD and (b) $Alq_3$ prepared at deposition rates of 0.01 and 1000 nm $s^{-1}$ and absorption coefficient−deposition rate characteristics of (c) α−NPD and (d) $Alq_3$.

**Fig. 5.** PL spectra of (a) α−NPD and (b) $Alq_3$ prepared at deposition rates of 0.01 and

1000 nm $s^{-1}$, PL quantum yield−deposition rate characteristics of (c) α−NPD and (d) $Alq_3$, PL lifetime−deposition rate characteristics of (e) α−NPD and (f) $Alq_3$, and PL radiative decay rate−deposition rate characteristics of (g) α−NPD and (h) $Alq_3$.

**Fig. 6.** Current density−voltage characteristics of (a) hole−only α−NPD devices and (b) electron−only $Alq_3$ devices and (c) current density−deposition rate characteristics at 1, 3, and 5 V (α−NPD) and at 10, 13, and 15 V ($Alq_3$) and TOF zero field hole mobility−deposition rate characteristics of α−NPD films..

**Fig. 7.** (a) TOF hole transients measured at electric field of $2.7\times10^5$ V $cm^{-1}$ and (b) hole mobility−square root of electric field characteristics of α−NPD prepared at different deposition rates.

**Fig. 8.** Polarized UV-vis absorption spectra of (a) α−NPD and (b) $Alq_3$ measured under normal and oblique light incidence. Deposition rates of α−NPD and $Alq_3$ are changed from 0.01 to 0.1, 1 and 10 nm $s^{-1}$.

**Fig. 9** (a) Current density−voltage and (b) external quantum efficiency−current density

characteristics of OLEDs prepared with different deposition rates and (c) drive voltage−deposition rate and external quantum efficiency−deposition rate characteristics at current densities of 1, 10, and 100 mA $cm^{-2}$.

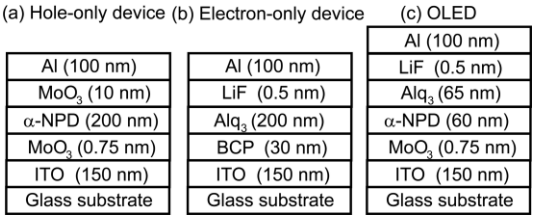


Fig. 1

Matsushima

Thin Solid Films

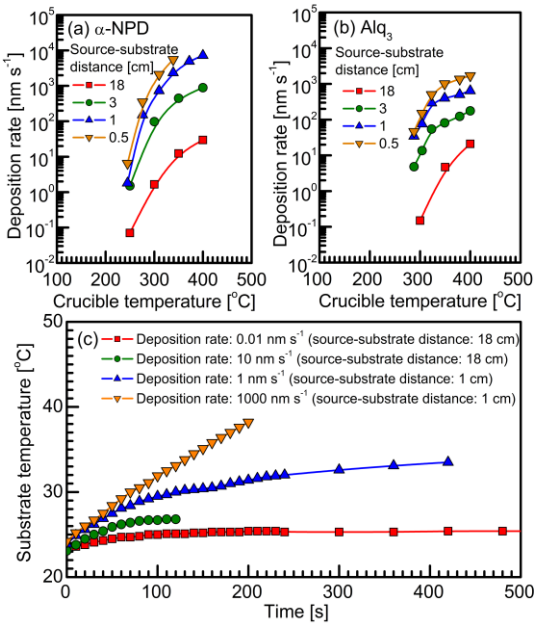


Fig. 2

Matsushima

Thin Solid Films

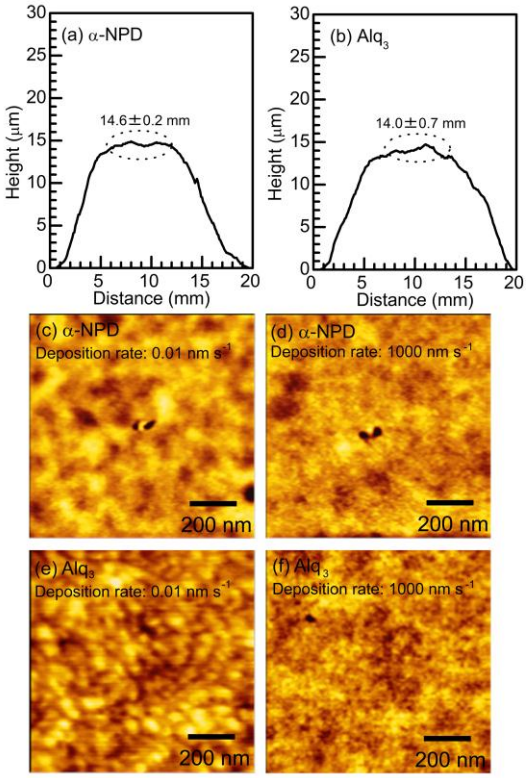


Fig. 3

Matsushima

Thin Solid Films

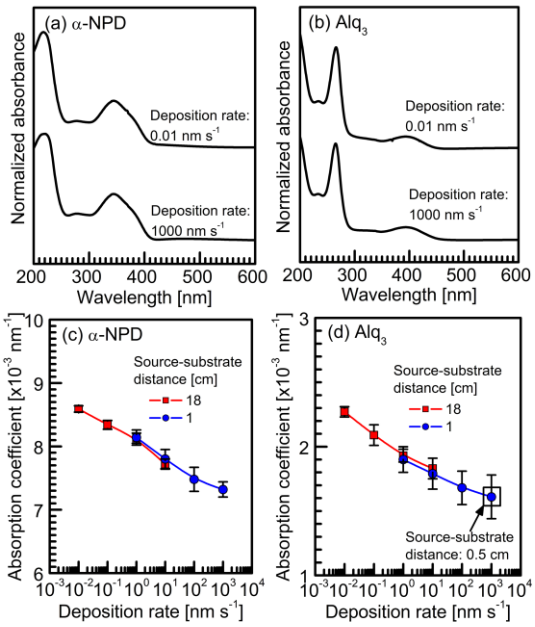


Fig. 4

Matsushima

Thin Solid Films

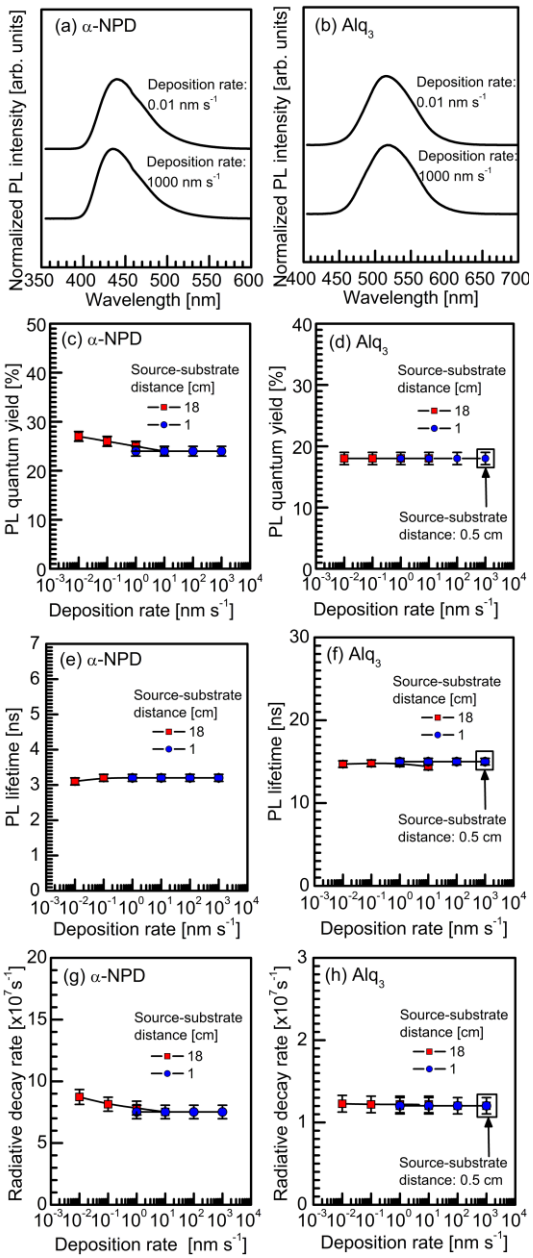


Fig. 5

Matsushima

Thin Solid Films

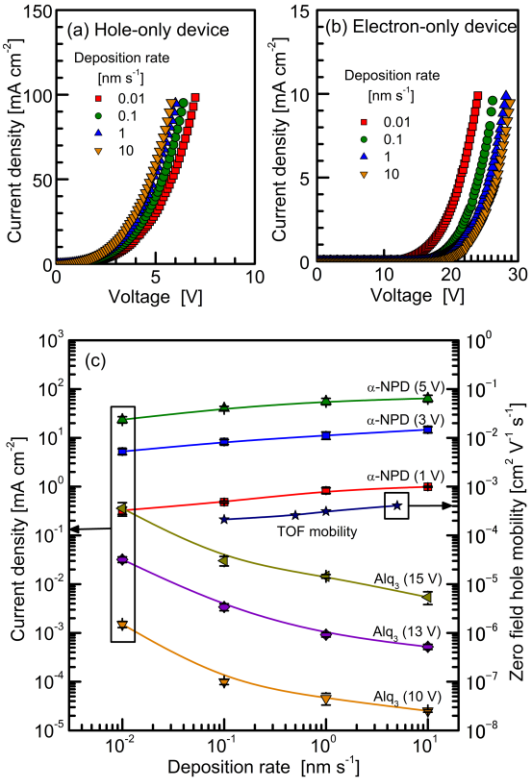


Fig. 6

Matsushima

Thin Solid Films

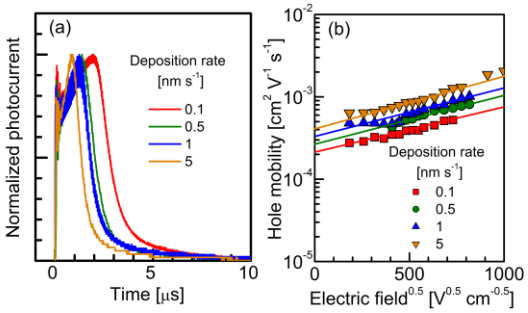


Fig. 7

Matsushima

Thin Solid Films

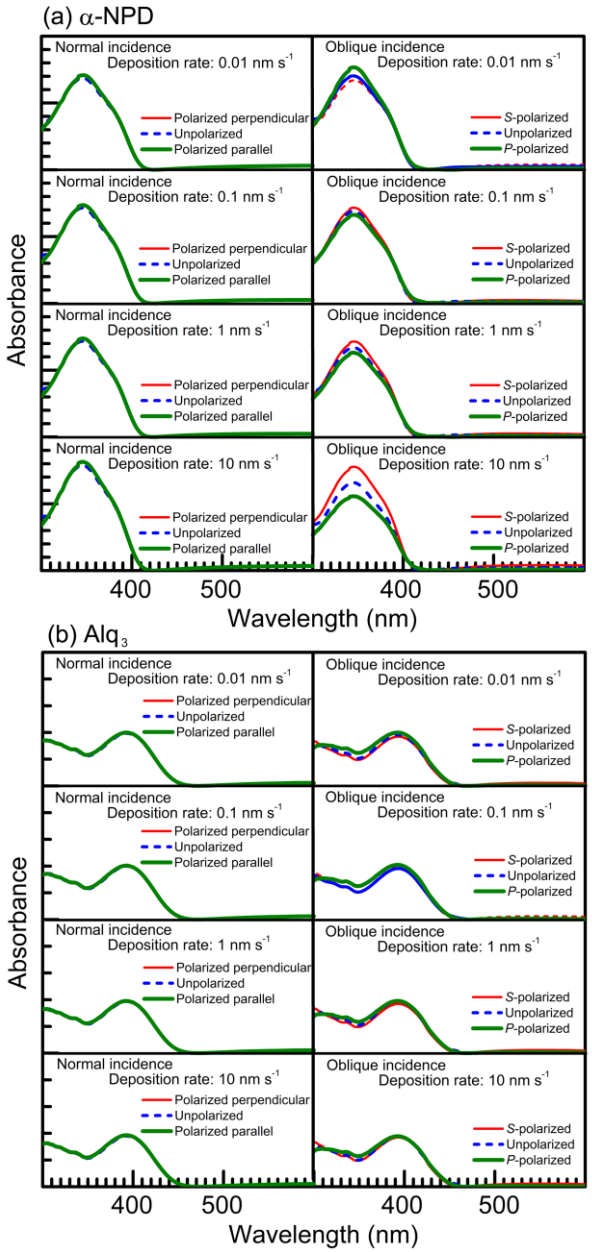


Fig. 8

Matsushima

Thin Solid Films

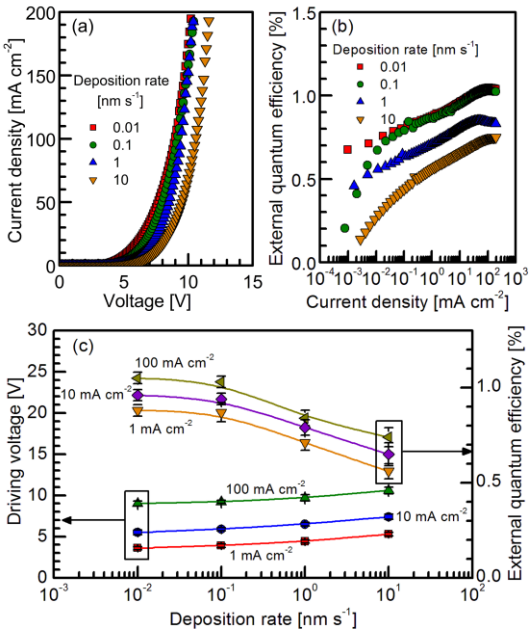


Fig. 9

Matsushima

Thin Solid Films